UC Davis

UC Davis Previously Published Works

Title

Significant Dzyaloshinskii–Moriya interaction at graphene–ferromagnet interfaces due to the Rashba effect

Permalink

https://escholarship.org/uc/item/4k5075n1

Journal

Nature Materials, 17(7)

ISSN

1476-1122

Authors

Yang, Hongxin
Chen, Gong
Cotta, Alexandre AC
et al.

Publication Date

2018-07-01

DOI

10.1038/s41563-018-0079-4

Peer reviewed

eScholarship.org Powered by the California Digital Library
University of California

Significant Dzyaloshinskii-Moriya Interaction at Graphene-Ferromagnet Interfaces due to Rashba-effect

Hongxin Yang[1,2,3 *,#], Gong Chen[4,5*,#], Alexandre A.C. Cotta[4,6,7,8], Alpha T. N'Diaye[4], Sergey A. Nikolaev[1], Edmar A. Soares[7], Waldemar A. A. Macedo[6], Kai Liu[5], Andreas K. Schmid[4,#], Albert Fert[2] & Mairbek Chshiev[1,#]

[1] Univ. Grenoble Alpes, CEA, CNRS, Grenoble INP, INAC-SPINTEC, 38000 Grenoble, France

[2] Unité Mixte de Physique, CNRS, Thales, Univ. Paris-Sud, Université Paris-Saclay, Palaiseau 91767, France

[3] Key Laboratory of Magnetic Materials and Devices, Ningbo Institute of Materials Technology and Engineering, Chinese Academy of Sciences, Ningbo, Zhejiang 315201, China

[4] NCEM, Molecular Foundry, Lawrence Berkeley National Laboratory, Berkeley, California 94720, USA

[5] Department of Physics, University of California, Davis, CA, 95616, USA

[6] Centro do Desenvolvimento da Tecnologia Nuclear, CDTN, 31270-901 Belo Horizonte, MG, Brazil

[7] Departamento de Física, ICEx, Universidade Federal de Minas Gerais, 31270-901 Belo Horizonte, MG, Brazil

[8] Present address: Departamento de Física, Universidade Federal de Lavras, 37200-000 Lavras, MG, Brazil

*These authors contributed equally to the work.

[#] To whom correspondence should be addressed.

E-mail: hongxin.yang.spintec@gmail.com, gchenncem@gmail.com, akschmid@lbl.gov, mair.chshiev@cea.fr

The possibility of utilizing the rich spin-dependent properties of graphene has attracted great attention in pursuit of spintronics advances. The promise of high-speed and low-energy consumption devices motivates a search for layered structures that stabilize chiral spin textures such as topologically protected skyrmions. Here we demonstrate that chiral spin textures are induced at graphene/ferromagnetic metal interfaces. Graphene is a weak spin-orbit coupling material and is generally not expected to induce sufficient Dzyaloshinskii-Moriya interaction to affect magnetic chirality. We demonstrate that indeed graphene induces a new type of Dzyaloshinskii-Moriya interaction due to a Rashba effect. First-principles calculations and experiments using spin-polarized electron microscopy show that this graphene-induced Dzyaloshinskii-Moriya interaction can have similar magnitude as at interfaces with heavy metals. This work paves a path towards two-dimensional material based spin orbitronics.

The unique properties of graphene including well-defined single atomic layer thickness, massless linear dispersion of its electronic structure, and long spin diffusion length have motivated the search for graphene-based phenomena that may enable spintronic applications[1,2,3]. Recently, graphene was shown to play key roles in several magnetic phenomena, including graphene-based tunnel magnetoresistance[4,5,6], enhancement of the spin-injection efficiency[7,8], Rashba effect[9,10], quantum spin Hall effect[11] and large perpendicular magnetic anisotropy (PMA)[12,13,14].

At the same time, recent progress in the field of spin orbitronics was stimulated by discoveries of phenomena permitting highly efficient electrical control of chiral spin textures, e.g. fast domain wall (DW) dynamics[15,16,17,18] and skyrmion motion at ultralow current densities[19,20,21,22]. These findings hold promise for applications in memory[23,24,25] and logic devices[26] where the interfacial Dzyaloshinskii-Moriya Interaction (DMI)[27,28] has been

recognized as a key ingredient in creation, stabilization, and manipulation of skyrmions[29,30,31,32,33,34] and chiral DWs[35,36]. While chiral magnetism induced by the interfacial DMI has become an important topic, the DMI at interfaces with graphene was not expected to be significant because, according to the Fert-Levy model[37], the DMI scales with spin-orbit coupling (SOC) in the material contacting the ferromagnetic metal (FM) layer[38] and graphene lacks strong SOC. Recent results reported the observation of enhanced PMA at the graphene/Co interface, even though strong interfacial PMA is also often associated with strong SOC[14,39]. This suggests that graphene/FM interfaces are unusual: if graphene enhances the PMA at interfaces in the absence of strong SOC, then it is interesting to ask if graphene has similarly strong effects on the DMI helping thereby to promote this and other 2D materials for spin orbitronics. In the following, this idea is tested by exploring the interfaces of graphene with cobalt and nickel, where these two FM elements are chosen for the small lattice mismatch and strong interaction with graphene.

First-principles calculations

The structures of graphene/FM films modelled here are shown in Fig. 1, where a layer of graphene coats the surfaces of three-monolayer (ML) thick hcp Co(0001) and fcc Ni(111) films. Arrows schematically indicate clockwise/right-handed and anticlockwise/left-handed (in parenthesis) spin spiral chirality. The calculated ground state structure is consistent with previous reports[4,14], where one carbon atom of the graphene unit cell is located on top of the adjacent Co(Ni) atom and another carbon atom is located above the hollow site, with the graphene/Co(Ni) distance of about 2.12 (2.15) Å.

We use the chirality dependent total energy difference approach applied previously for Co/Pt structures[33,38,40] to calculate microscopic and micromagnetic DMI constants, d^{tot} and D, respectively, as well as the layer-resolved DMI, d^k, where k indicates the individual

atomic layers within FM films. As one can see from Fig. 2 for the calculated results, the largest DMI can reach up to 1.14 meV per atom for a graphene coated single atomic layer of Co, while for 2 and 3 ML of Co films coated by graphene, the amplitude of d^{tot} drops to 0.16 and 0.49 meV, respectively (Fig. 2a). Moreover, d^{tot} of graphene/Co (brown bars in Fig.2a) is generally stronger than that of graphene/Ni (green bars in Fig. 2a) for all thicknesses considered. For the micromagnetic DMI, D, we found that its magnitude decreases as a function of the FM layer thickness for both graphene coated Co and Ni films, due to interfacial origin of the DMI leading to the inverse proportionality with respect to FM layer thickness.[38]

In order to elucidate the origin of such a significant DMI in graphene coated FM, we then calculated the layer-resolved DMI, d^k, and associated SOC energy difference, $\Delta E_{\mathrm{SOC}}^k$, for the case of graphene coated 3ML Co films. Fig. 2c shows that the largest layer-resolved DMI, d^k, is located at the interfacial Co layer, labelled as Co1 (blue bar), which is in contact with graphene, while within the layers further from the interface the DMI decays very fast (red and black bars), similar to previously reported case at Co/Pt interface[38]. However, significant differences between graphene/Co and Co/Pt emerge in terms of where the corresponding SOC energy source is located. As shown in Fig. 2d, the largest associated SOC energy difference, $\Delta E_{\mathrm{SOC}}^k$, originates from the same Co1 layer rather than from the non-magnetic side of the interface, where it is almost zero. This is drastically different from the Co/Pt case where the SOC energy difference is mainly contributed by the adjacent Pt layer. These findings indicate that the physical mechanism governing the strength of the DMI in graphene/Co interface is very different from that in Co/Pt, which is captured by the Fert-Levy model[37,38]. Instead, in graphene/Co the dominating mechanism is the Rashba-type DMI. According to the latter[41,42,43], the DMI parameter can be roughly expressed as $d = 2k_{\mathrm{R}}A$ at

graphene/Co interfaces, where A is the exchange stiffness and $k_R = \frac{2\alpha_R m_e}{\hbar^2}$ is determined by the Rashba coefficient, α_R, and effective electron mass, m_e. The latter in Co was measured to be about 0.45 m_0[44] (with m_0 being the rest mass of electron), and the exchange stiffness, A, was found to be about 9.5 pJ/m for graphene/Co (3ML)/Ru(0001) based on the Curie temperature of this structure (see details in Method), which is slightly smaller than A=15 pJ/m in thicker Co films[34,45]. The Rashba coefficient, α_R, can then be extracted from $\alpha_R=2E_0/k_0$, where E_0 is the Rashba splitting at the wave vector k_0. We calculated the Rashba splitting for graphene/Co(3ML) slab by switching on SOC and putting the magnetization along <11$\bar{2}$0> and <$\bar{1}\bar{1}$20>. As one can see in Figs. 2e and f, the corresponding band shifts are a signature of the Rashba effect even though it deviates slightly from the conventional linear dependence given by α_R (**σ** x **k**)·**z.** Different characters of the band splitting at the $\bar{\Gamma}$ point can be attributed to the fact that Co d orbitals are influenced by different potential gradients due to the polarization between graphene and Co that provides an intrinsic electric field and considerably enhances the effective value of SOC at the interface. We chose a band close to the Fermi level at $\bar{\Gamma}$ point, as shown in Fig. 2f, to estimate the Rashba-type DMI. The Rashba splitting, E_0, is about 1.28 meV at k_0=0.031 Å^{-1}, and the Rashba coefficient, α_R is thus found to be about 82.6 meV· Å. This leads to k_R=9.8×10^{-3} Å^{-1} and therefore d=0.18 meV at graphene/Co interfaces, which is smaller than the value calculated from first-principles, d=0.49 meV for graphene coated 3 ML Co films. The reason for the smaller DMI value extracted from the Rashba effect can be ascribed to the fact that the Rashba-type DMI was estimated by using only one band close to the Fermi level. As reported in recent studies[46], the magnitude and sign of α_R is generally band-dependent due to band-specific orbital orderings of the orbital angular momentum giving rise to the band-dependent orbital chirality.

Experimental observation of graphene-induced DMI

Experimental tests of the DMI were done using spin-polarized low-energy electron microscopy (SPLEEM), by directly imaging DWs in perpendicularly magnetized films (see Methods). The films were prepared *in-situ* by molecular beam epitaxy under ultrahigh vacuum conditions so that possible extrinsic influences such as growth front roughness are minimal and controlled[47]. The sign of the DMI can be determined by observing the chirality of DWs[32,36,48], while the strength of the DMI vector, d, can be quantified by measuring the film thickness dependence of a transition from chiral Néel walls (in thin films, where the interfacial DMI influences DW texture) to achiral Bloch walls (in thicker films, where dipolar forces outweigh the DMI)[36,48]. We cannot prepare a free standing graphene/Co bilayer where the thickness of Co is several ML, instead, high quality graphene/Co samples were prepared on top of Ru(0001) single-crystal substrates (see Methods).

Figs. 3a,b show compound SPLEEM images highlighting the DW spin structure in graphene/Co/Ru(0001) films, where black and grey shades indicate that the magnetization is perpendicular to the film plane with $+M_z$ and $-M_z$ vectors, respectively, while colours represent the in-plane magnetization vector according to the colour wheel (inset). For Co thickness of 3.9 ML (Fig. 3a) the in-plane component of the magnetization within DWs (white arrows) is perpendicular to the DW tangent, and always points from grey domains to black domains, i.e. from $-M_z$ and $+M_z$: this indicates that the DWs have a left-handed/anti-clockwise chiral Néel texture[36,48]. For Co thickness of 8.4 ML (Fig. 3b), the magnetization vector within DWs is aligned parallel to the DW tangent: this indicates that the DW has a Bloch-type texture. Moreover, the magnetization vector within these DWs reverses its direction in a number of places, indicating that these DWs are achiral Bloch-walls[49]. This thickness-dependent transition of the DW type and chirality can be tracked in more detail

using histogram as plotted in Fig. 3c (see Methods). The histogram represents the distribution of the angle α, defined as the angle between the DW magnetization vector **m** and the normal direction of DW, **n** (Fig. 3c inset). The distribution of the angle α gradually evolves from a single peak around 0^{o} for Co 3.9 ML to double peaks at ±90° for Co 8.4 ML thicknesses.

The strength of the DMI in this system can be estimated as d=0.11±0.04 meV per atom (Fig. 3f), by computing the film thickness related dipolar energy difference between Néel- and Bloch- textured DWs. Note that this analysis is independent of the values of exchange interaction and magnetic anisotropy in a given system (see Methods). The DMI parameter d contains contributions from both the graphene/Co interface and the Co/Ru interface, and the DMI at Co/Ru needs to be tested so that the DMI at graphene/Co can be deduced. In the Co/Ru(0001) system, a spin reorientation transition from out-of-plane to in-plane occurs from 2ML Co to 3ML Co coverage[50]. The step-flow growth mode of this system permits deposition of a Co film of 2.4ML coverage that consists of alternating strips of 2ML and 3ML thickness, featuring out-of-plane- and in-plane domains with well-defined areas (Supplementary Fig. S1). Analogous to Ref. 51, the magnetic structure of this sample is an inhomogeneous spin spiral. SPLEEM imaging (Fig. 3d) and analysis of histograms of the domain wall magnetization angle α indicates that the Co/Ru system features right-handed Néel-type chirality. In detail, the split double peak near $\alpha = 180^{\circ}$ in the histogram plotted in Fig. 3e indicates DW spin textures point roughly 45° with respect to the domain boundary, where the DMI energy is comparable to the dipolar energy difference between Néel- and Bloch- textured DWs. From this observation the DMI at Co/Ru can be estimated as $d = -0.05 \pm 0.01$ meV per atom (see Methods). The DMI is very localized at the interface[38,40], and in both Co/Ru and graphene/Co/Ru samples the Co layer is either pseudomorphic (hcp, for 1 ML Co thickness) or a moiré structure chiefly composed of alternating fcc and hcp

regions (for 2 ML or larger Co thickness, see details in Methods). From the experimental DMI values of Graphene/Co/Ru and Co/Ru, the DMI of the Graphene/Co interface with 4-6ML Co can be determined to be $d = 0.16 \pm 0.05$ meV per atom (Fig. 3f) (see more details in Methods), which is opposite and about three times as strong as the DMI at the Co/Ru interface. This is consistent with the calculated DMI of $d = 0.18$ meV for Graphene/Co[3ML] based on the Rashba model discussed above.

Towards a giant DMI in graphene-based heterostructures

It was previously proposed that the DMI can be amplified using multilayer structures[34,36,40,52]. As summarized in Fig. 2, the sign of the DMI for graphene/Ni with Ni thickness of 1 and 2 MLs is negative (clockwise/right-handed chirality), while for graphene/Co the sign is always positive (anticlockwise/left-handed chirality). This suggests the possibility to obtain large DMI values by building ternary superlattices based on graphene/Co/Ni heterostructures. We tested this hypothesis with first-principles calculations by modelling graphene/[Co/Ni/graphene]$_n$ structures (Fig. 4). The calculated value of d increases with respect to the number of repeating units, n, with a slope less than one. Further calculations indicate that the amplification of the DMI can be further enhanced in Van der Waals heterostructures where two FM layers are separated by two MLs of graphene, i.e. in multilayers of the graphene/[Co/Ni/bilayer-graphene/]$_{(m\text{-}1)}$/Co/Ni/graphene structure. The result obtained for m=2 with $d = 1.13$ meV suggests that in multilayers of n repeating units the DMI approaches a value of m times the DMI of a single graphene/Co/Ni/graphene unit. Furthermore, calculating the PMA for graphene/[Co/Ni/graphene]$_n$ heterostructures shows a linear increase with the number of repeating units n, that is similar to the behaviour of graphene/[Co/graphene]$_n$ reported before[14].

From the values of the DMI at Co/graphene interfaces obtained in this work, we

predict that graphene induced DMI should be sufficient to stabilize magnetic chiral spin textures in ultrathin FM films attached to graphene. For instance, magnetic chiral DWs and skyrmions have been observed in weak DMI systems (-0.12 meV per atom at Ni/Ir interface[48], or 0.15 meV per atom in Fe/Ni/Cu system[36]). The proposed [Co/Ni/graphene]$_n$ heterostructure allows simultaneous enhancement of the DMI and PMA, which may be helpful for stabilizing chiral spin textures such as skyrmions with an extremely small size. Moreover, graphene/Co(Ni) grown on copper could be interesting since graphene production on copper is a well-established process[53], where the graphene related interface is expected to dominate the DMI due to the ignorable DMI at Co(Ni)/Cu interface[52].

In summary, we have discovered both from first-principles calculations and from magnetic imaging experiments that graphene/FM interface generates significant DMI. We showed that the physical origin of this DMI is the Rashba-effect. The discovery of the DMI induced by graphene along with its distinctive electronic properties[54], enhancement of PMA[14], and its ability to act as an excellent capping layer[55], may open up a new area in the field of spintronics.

ACKNOWLEDGEMENTS

This work was supported by the European Union's Horizon 2020 Research and Innovation Programme under grant agreement No. 696656 (GRAPHENE FLAGSHIP), the ANR ULTRASKY, SOSPIN. *Ab initio* calculations used resource of GENCI-CINES with grant No. C2016097605. Work at the Molecular Foundry was supported by the Office of Science, Office of Basic Energy Sciences, of the U.S. Department of Energy under Contract No. DE-AC02-05CH11231. Work at UCD was supported by the UC Office of the President Multicampus Research Programs and Initiatives MRP-17-454963 (G.C.) and NSF DMR-1610060 (K.L.). A.A.C.C., W.A.A.M. and E.A.S. acknowledge the support of Brazilian

agencies CAPES, CNPq and FAPEMIG. H.X.Y. would like also to acknowledge the 1000 Talents Program for Young Scientists of China and Ningbo 3315 Program. We thank V. Cros, O. Boulle, G. Gaudin, I. M. Miron, T. P. Ma and A. Thiaville for fruitful discussions and comments.

AUTHOR CONTRIBUTIONS

H.X.Y. and G.C. conceived the study. H.X.Y and S.A.N. performed the *ab-initio* calculations with help of M.C. H.X.Y., M.C., S.A.N. and A.F. analyzed and interpreted the *ab-initio* results. G.C. and A.A.C.C. carried out the SPLEEM measurements. A.K.S. supervised the SPLEEM facility. G.C., A.A.C.C., A.T.N., K.L., A.K.S analyzed the SPLEEM results. G.C. derived DMI strength from experimental data. G.C., A.A.C.C., A.T.N., K.L., A.K.S., E.A.S, W.A.A.M., interpreted and discussed the experimental result. A.A.C.C., E.A.S, W.A.A.M. performed XPS measurement. H.X.Y and G.C. prepared the manuscript with help from A.A.C.C., A.K.S., S.A.N. and M.C. All authors commented on the manuscript.

COMPETING INTERESTS STATEMENT

The authors declare that they have no competing financial interests.

Figure Captions

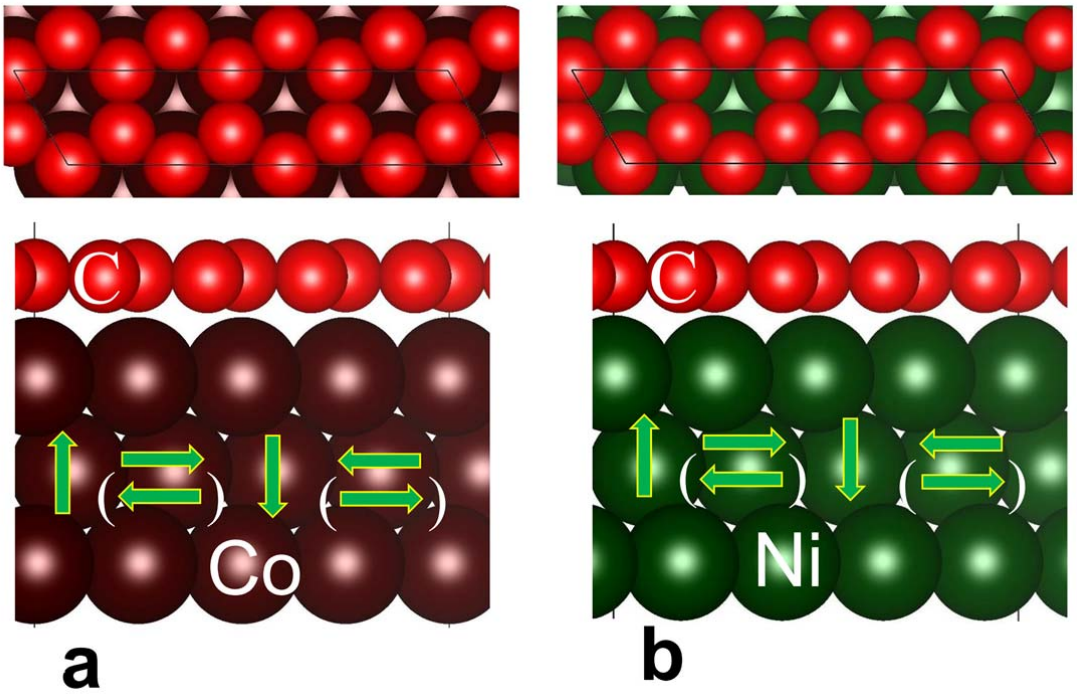

Figure 1 Crystal and spin configurations of graphene coated Co and Ni films used for DMI calculations. a, Top- and side-view of graphene on hcp Co(0001) and **b**, top- and side-view of graphene on fcc Ni(111) surface. Red, purple and green balls represent carbon, cobalt and nickel atoms, respectively. Clockwise (anticlockwise) spin configurations are schematically shown by arrows.

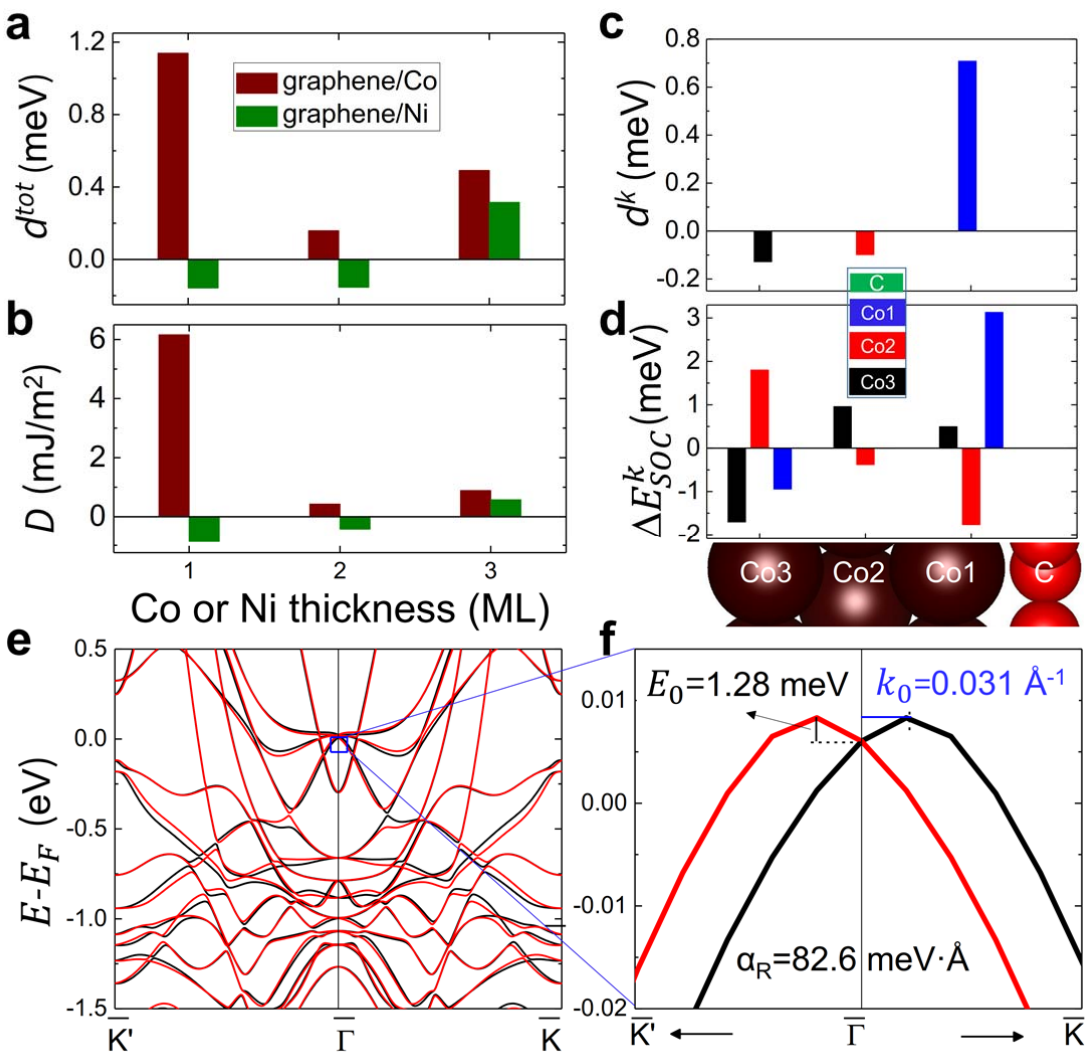

239 **Figure 2 Anatomy of DMI for graphene/Co and graphene/Ni bilayers. a,** Total DMI
240 coefficient d^{tot} and **b,** micromagnetic DMI coefficient D, as a function of FM film thickness
241 for graphene/Co (brown bars) and graphene/Ni (green bars) slabs. **c,** Layer-resolved DMI
242 coefficient d^k of the k^{th} layer for graphene/Co(3ML) slab. **d,** Atomic layer resolved
243 localization of the associated spin-orbit energy ΔE^k_{SOC}. As it is seen, the large DMI coefficient
244 of the Co1 layer (blue bar in **c**) is associated with large variations of the SO energy ΔE^{Co1}_{SOC} in
245 the Co1 layer (see the corresponding blue bar in **d**). **e** and **f**, Band structures for
246 graphene/Co(3ML) slab with the magnetization axis along <11$\bar{2}$0> (black) and <$\bar{1}\bar{1}$20> (red)
247 used to estimate the Rashba splitting. The corresponding DMI is found to be about 0.18 meV.

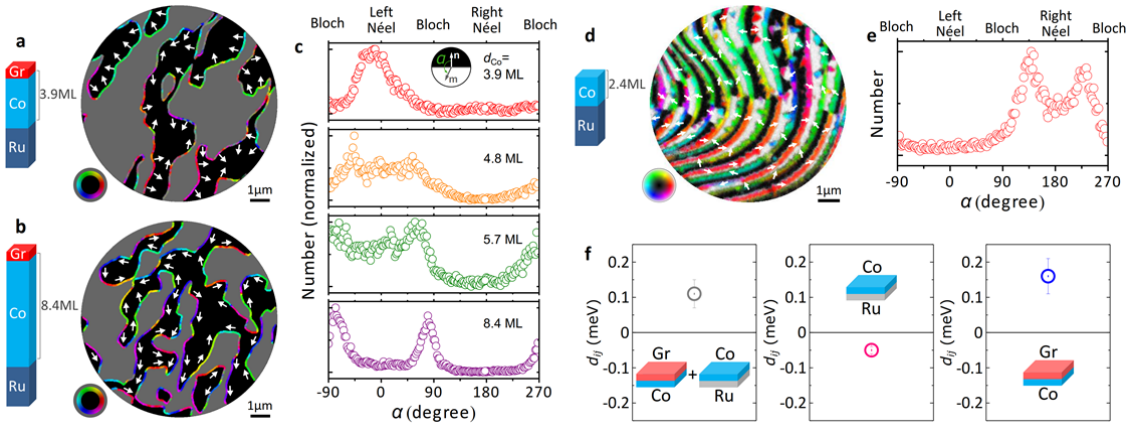

Figure 3 Experimental measurement of DMI in graphene/Co by using SPLEEM. a,b, Compound SPLEEM images of graphene/Co/Ru. Scale bar, 1μm. White arrows indicate the orientation of in-plane magnetization. **c,** Co thickness dependent histogram of the angle α counted pixel-by-pixel at the DW boundary in graphene/Co/Ru(0001) shows the evolution of the chirality from a left-handed Néel wall (single peak at 0°) to an achiral Bloch wall (double peaks at ±90°). Inset shows the definition of the angle α, where **m** is the in-plane direction of the DW magnetization, and **n** is the in-plane vector normal to the domain boundary and always points from grey domains to black domains. **d,** Compound SPLEEM image of Co/Ru. Scale bar, 1μm. **e,** the angle α histogram in Co/Ru indicates right-handed Néel-type rotation. **f,** Calculated DMI vector $\boldsymbol{d}_{ij}$ strength.

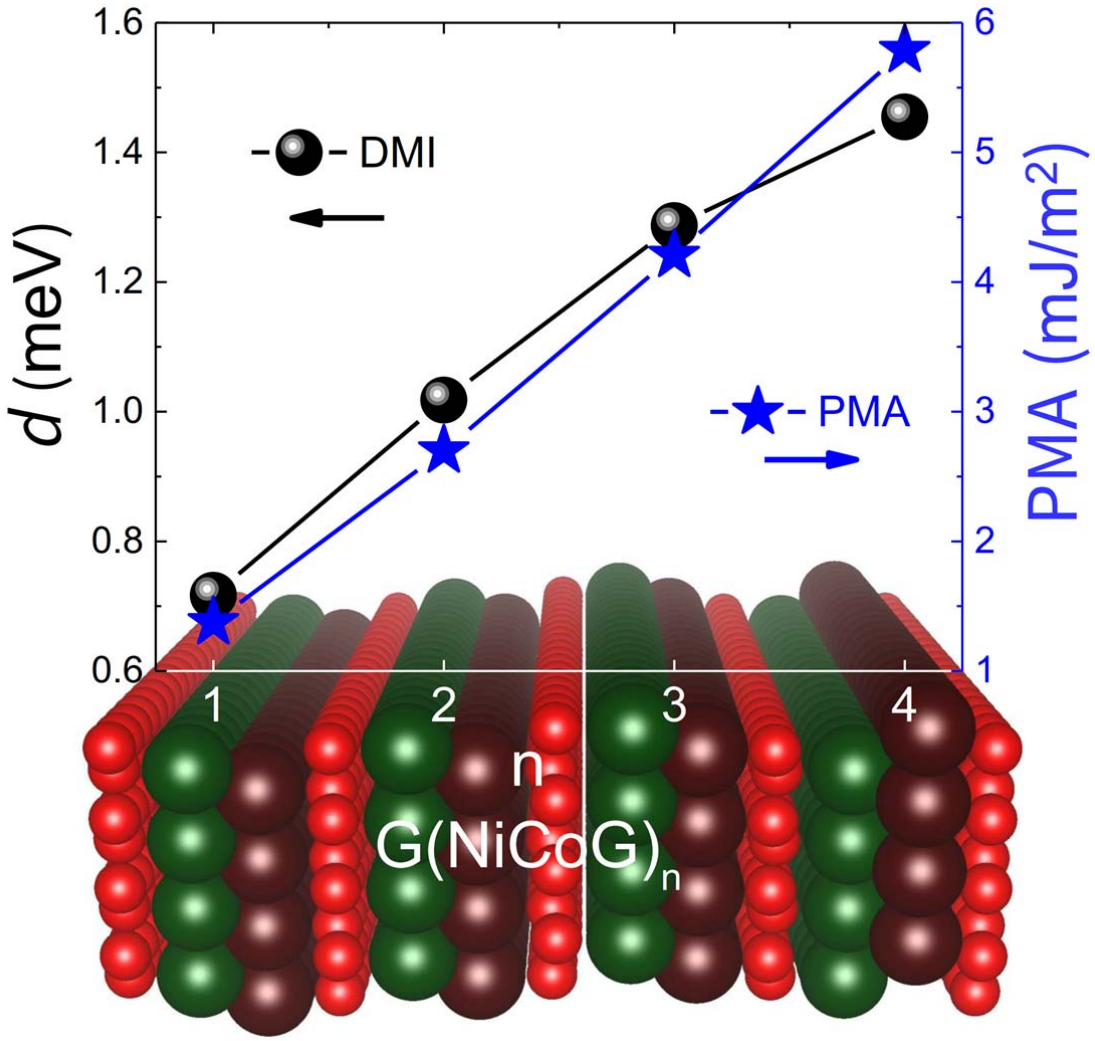

259 **Figure 4 DMI and PMA for the multilayer of graphene/[Co/Ni/graphene]$_n$ as a function**
260 **of the junction number *n*.** Black points pointing to the left scale and blue stars pointing to
261 the right scale represent the calculated DMI and PMA values, respectively. Both the DMI and
262 PMA increase approximately linearly as a function of the junction number *n*. The atoms
263 represented by different colours are the same as in Figure 1.
264

[1] Castro Neto, A. H., Guinea, F., Peres, N. M. R., Novoselov, K. S. & Geim, A. K. The electronic properties of graphene. *Rev. Mod. Phys.* **81**, 109–162 (2009).
[2] Han, W., Kawakami, R. K., Gmitra, M. & Fabian, J. Graphene spintronics. *Nat. Nanotech.* **9**, 794–807 (2014).
[3] Roche, S. et al. Graphene spintronics: the European Flagship perspective. *2D Materials* **2**, 030202 (2015).
[4] Karpan, V. M. et al. Graphite and Graphene as Perfect Spin Filters. *Phys. Rev. Lett.* **99**, 176602 (2007)
[5] Cobas, E., Friedman, A. L., van't Erve, O. M. J., Robinson, J. T. & Jonker, B. T. Graphene As a Tunnel Barrier: Graphene-Based Magnetic Tunnel Junctions. *Nano Lett.* **12**, 3000–3004 (2012).
[6] Bodepudi, S. C., Singh, A. P. & Pramanik, S. Giant Current-Perpendicular-to-Plane Magnetoresistance in Multilayer Graphene as Grown on Nickel. *Nano Lett.* **14**, 2233 (2014).
[7] Han, W. et al. Tunneling spin injection into single layer graphene. *Phys. Rev. Lett.* **105**, 167202 (2010).
[8] Dlubak, B. et al. Highly efficient spin transport in epitaxial graphene on SiC. *Nat. Phys.* **8**, 557–561 (2012).
[9] Dedkov, Yu. S., Fonin, M., Rüdiger, U. & Laubschat, C. Rashba Effect in the Graphene/Ni(111) System. *Phys. Rev. Lett.* **100**, 107602 (2008).
[10] Liu, M.-H., Bundesmann, J. & Richter, K. Spin-dependent Klein tunneling in graphene: Role of Rashba spin–orbit coupling. *Phys. Rev. B* **85**, 085406 (2012).
[11] Kane, C. L. & Mele, E. J. Quantum spin Hall effect in graphene. *Phys. Rev. Lett.* **95**, 226801 (2005).
[12] Vo-Van, C. et al. Ultrathin epitaxial cobalt films on graphene for spintronic investigations and applications, *New J. Phys.* **12**, 103040 (2010)
[13] Rougemaille, N. et al. Perpendicular magnetic anisotropy of cobalt films intercalated under graphene, *Appl. Phys. Lett.* **101**, 142403 (2012)
[14] Yang, H. X. et al. Anatomy and Giant Enhancement of the Perpendicular Magnetic Anisotropy of Cobalt-Graphene Heterostructures. *Nano Lett.* **16**, 145 (2015).
[15] Miron, I. M. et al. Fast current-induced domain-wall motion controlled by the Rashba effect. *Nat. Mater*. **10**, 419–423 (2011).
[16] Emori, S., Bauer, U., Ahn, S.-M., Martinez, E. & Beach, S. D. Current-driven dynamics of chiral ferromagnetic domain walls. *Nat. Mater*. **12**, 611 (2013).
[17] Ryu, K.-S., Thomas, L. Yang, S.-H. & Parkin, S. Chiral spin torque at magnetic domain walls. *Nat. Nanotech*. **8**, 527 (2013).
[18] Haazen, P. P. J. et al. Domain wall depinning governed by the spin Hall effect. *Nat. Mater*. **12**, 299 (2013).
[19] Jonietz F. et al. Spin Transfer Torques in MnSi at Ultralow Current Densities. *Science* **330**, 1648-1651 (2010)
[20] Romming, N. et al., Writing and Deleting Single Magnetic Skyrmions. *Science* **341**, 634 (2013).
[21] Yu, X.Z. et al., Skyrmion flow near room temperature in an ultralow current density. *Nat. Communications* **3**, 988 (2012).
[22] Iwasaki, J., Mochizuki, M. & Nagaosa, N. Current-induced skyrmions in constricted geometries. *Nat. Nanotech*. **8**, 742 (2013).

[23] Parkin, S. S. P., Hayasi, M. & Thomas, L. Magnetic Domain-Wall Racetrack Memory. *Science* **320**, 197202 (2009).
[24] Fert, A., Cros, V. & Sampaio, J. Skyrmions on the track. *Nat. Nanotech.* **8**, 152–156 (2013).
[25] Nagaosa, N. & Tokura, Y. Topological properties and dynamics of magnetic skyrmions. *Nat. Nanotech*. **8**, 899–911 (2013).
[26] Allwood, D. A., et al. Magnetic domain-wall logic. *Science* **309**, 1688-1692 (2005).
[27] Dzyaloshinskii, I. E. *Sov. Phys. JETP* **5**, 1259 (1957).
[28] Moriya, T. Anisotropic superexchange interaction and weak Ferromagnetism. *Phys. Rev.* **120**, 91–98 (1960).
[29] Yu, X. Z. et al. Real-space observation of a two-dimensional skyrmion crystal. *Nature* **465**, 901–904 (2010).
[30] Sampaio, J., Cros, V., Rohart, S., Thiaville, A. & Fert, A. Nucleation, stability and current-induced motion of isolated magnetic skyrmions in nanostructures. *Nat. Nanotech.* **8**, 839–844 (2013).
[31] Jiang, W. et al. Blowing magnetic skyrmion bubbles. *Science* **349**, 283 (2015).
[32] Chen, G. et al. Room temperature skyrmion ground state stabilized through interlayer exchange coupling. *Appl. Phys. Lett*. **106**, 242404 (2015).
[33] Boulle, O. et al. Room-temperature chiral magnetic skyrmions in ultrathin magnetic nanostructure. *Nat. Nanotech*. **11**, 449 (2016).
[34] Moreau-Luchaire, C. et al. Additive interfacial chiral interaction in multilayers for stabilization of small individual skyrmions at room temperature. *Nat. Nanotech.* **11**, 444 (2016).
[35] Thiaville, A., Rohart, S., Jué, É., Cros, V. & Fert, A. Dynamics of Dzyaloshinskii domain walls in ultrathin magnetic films. *Europhys. Lett.* **100**, 57002 (2012).
[36] Chen, G. et al. Novel Chiral Magnetic Domain Wall Structure in Fe/Ni/Cu(001) Films. *Phys. Rev. Lett*. **110**, 177204 (2013).
[37] Fert, A. & Levy, P. M. Role of Anisotropic Exchange Interactions in Determining the Properties of Spin-Glasses. *Phys. Rev. Lett*. **44**, 1538–1541 (1980)
[38] Yang, H., Thiaville, A., Rohart, S., Fert, A. & Chshiev, M. Anatomy of Dzyaloshinskii–Moriya interaction at Co/Pt interfaces. *Phys. Rev. Lett.* **115**, 267210 (2015).
[39] Dieny, B. & Chshiev, M. Perpendicular magnetic anisotropy at transition metal/oxide interfaces and applications, *Rev. Mod. Phys.* **89**, 025008 (2017).
[40] Yang, H. X., Boulle, O., Cros, V., Fert, A. & Chshiev, M. Controlling Dzyaloshinskii-Moriya Interaction via Chirality Dependent Layer Stacking, Insulator Capping and Electric Field. *arXiv*:1603.01847 (2016).
[41] Kundu, A. and Zhang, S. Dzyaloshinskii-Moriya interaction mediated by spin-polarized band with Rashba spin-orbit coupling. *Phys. Rev. B* **92**, 094434 (2015).
[42] Imamura, H., Bruno, P. and Utsumi, Y. Twisted exchange interaction between localized spins embedded in a one- or two-dimensional electron gas with Rashba spin-orbit coupling. *Phys. Rev. B* **69**, 121303(R) (2015).
[43] Kim, K.-W., Lee, H.-W., Lee, K.-J. & Stiles, M. D. Chirality from interfacial spin-orbit coupling effects in magnetic bilayers. *Phys. Rev. Lett.* **111**, 216601 (2013).
[44] Bode, S., Starke, K. & Kaindl, G. Spin-dependent surface band structure of hcp Co(10$\bar{1}$0). *Phys. Rev. B* **60**, 2946 (1999).

[45] Eyrich, C. et al. Effects of substitution on the exchange stiffness and magnetization of Co films. *Phys. Rev. B* **90**, 235408 (2014).
[46] Park, J.-H. et al. Orbital chirality and Rashba interaction in magnetic bands. *Phys. Rev. B* **87**, 041301(R) (2013).
[47] Lee-Hone, N. R., et al. Roughness-induced domain structure in perpendicular Co/Ni multilayers. arXiv:1612.04867 (2016).
[48] Chen, G. et al. Tailoring the chirality of magnetic domain walls by interface engineering. *Nat. Commun.* **4**, 2671 (2013).
[49] Chen, G. et al. Unlocking Bloch-type chirality in ultrathin magnets through uniaxial strain. *Nat. Commun*. **6**, 6598 (2015).
[50] El Gabaly, F. et al. Imaging spin-reorientation transitions in consecutive atomic Co layers on Ru (0001). *Phys. Rev. Lett.* **96** (14), 147202 (2006)
[51] Meckler, S. et al. Real-space observation of a right-rotating inhomogeneous cycloidal spin spiral by spin-polarized scanning tunneling microscopy in a triple axes vector magnet. Phys. Rev. Lett. **103**, 157201 (2009).
[52] Chen, G. et al. Ternary superlattice boosting interface-stabilized magnetic chirality. *Appl. Phys. Lett*. **106**, 062402 (2015).
[53] Li, X. et al. Large-Area Synthesis of High-Quality and Uniform Graphene Films on Copper Foils. *Science* **324**, 1312-1314 (2009).
[54] Geim, A. K. & Novoselov, K. S. The rise of graphene. *Nat. Mater.* **6**, 183 - 191 (2007).
[55] Coraux, J. et al. Air-protected epitaxial graphene/ferromagnet hybrids prepared by chemical vapor deposition and intercalation. *J. Phys. Chem. Lett.* **3**, 2059-2063 (2012).

METHODS

First-principles calculations. The Vienna *ab initio* simulation package (VASP) was used in our calculations with electron-core interactions described by the projector augmented wave method, and the exchange correlation energy calculated within the generalized gradient approximation of the Perdew-Burke-Ernzerhof (PBE) form[56,57]. The cutoff energies for the plane wave basis set used to expand the Kohn-Sham orbitals were chosen to be 520 eV for all calculations. The Monkhorst-Pack scheme was used for the Γ-centred 4×16×1 *k*-point mesh. In order to extract the DMI vectors, the calculations were performed in three steps. First, the corresponding structures were relaxed until the forces become smaller than 0.001 eV/Å to determine the most stable interfacial geometries. In our DMI calculations, we coated 1 to 3 monolayers of hcp Co(0001) or fcc Ni(001) films by graphene in a 4 by 1 surface unit cell with $\pi/2$ spin rotations (Fig. 1), we also calculated hcp- or fcc stacked Co films on bare Ru(0001) in same unit cell. Next, the Kohn-Sham equations were solved with no spin-orbit interaction taken into account to find out the charge distribution of the system's ground state. Finally, spin-orbit coupling was included and the self-consistent total energy of the systems was determined as a function of the constrained magnetic moments. We employ the same method used for DMI calculations in frustrated bulk systems and insulating chiral-lattice magnets[58] and adapted to the case of interfaces. As for the Rashba effect, we adopted the same approach as in Ref. [59] (see also Supplementary Fig. S.2 and corresponding discussion).

Sample preparation. We conducted the experiments in the SPLEEM system at National Center for Electron Microscopy of Lawrence Berkeley National Laboratory. All samples were prepared under ultra-high vacuum (UHV) conditions, with base pressure better than 4.0×10^{-11} Torr. Ru(0001) substrates were cleaned by repeated flash annealing at 1470 K in

289 $3.0x10^{-8}$ Torr O^2 atmosphere and final annealing at 1430 K under UHV. After such
290 procedure, we did not observe any trace of contaminants by Auger electron spectroscopy
291 (AES) and LEEM. Furthermore, high-quality low energy electron diffraction patterns were
292 obtained, indicating a well-ordered surface.

293 Graphene was grown by chemical vapour deposition method[55], where we kept the
294 substrate at 920 K under ethylene atmosphere (10^{-8} Torr) for around 15 minutes, while
295 observing the process by LEEM. Preparing graphene at low growth temperature is required
296 for a good intercalation process, since defects within the graphene layer assist the cobalt
297 migration. The presence of graphene was confirmed by the moiré pattern in low energy
298 electron diffraction[60] (see Supplementary Fig. S.3). After cooling graphene/Ru(0001) to
299 room temperature, an amount of one monolayer Co was deposited by electron beam
300 evaporation at rates of 0.18 ML per minute, and intercalated by annealing at 620 K for 3
301 minutes[61]. In order to achieve higher Co thicknesses, we repeated the intercalation of
302 additional monolayer-doses of Co, exploring layer thicknesses up to 24 ML Co. The Co
303 growth rate was calibrated by monitoring the LEEM image intensity during the deposition of
304 Co directly onto bare Ru (0001). For the Co/Ru films, Co layers were deposited on Ru(0001)
305 by electron beam evaporation at 460 K substrate temperature, promoting step flow growth
306 mode. The atomic layer thickness of the Co deposit is known directly from monitoring the
307 step flow growth in-situ in LEEM.

308 The growth of magnetic layers was monitored by low-energy electron diffraction
309 (LEED). All of the samples show sharp diffraction patterns, indicating well-defined
310 crystallinity and epitaxy (see Supplementary Fig. S.4). The 1st Co layer grows
311 pseudomorphic on clean Ru, consistent with Ref. 62. In the presence of graphene, the
312 pseudomorphic structure of one monolayer Co between graphene and Ru(0001) has been

reported by scanning tunneling microscopy in Ref. 61 and Ref. 63, where the structure of the graphene moiré pattern remains identical before and after the intercalation of the first monolayer Co, proving that the Co monolayer under the graphene is pseudomorphic with the Ru(0001). For thicker Co coverages, superstructures near the first-order LEED spots (see example in Supplementary Fig. S.4e) have been attributed to relaxation of the lattice mismatch between Co and Ru, resulting in an epitaxial relationship that features Co layers with essentially bulk structure, where lattice mismatch strain is relieved at the Co/Ru interface in a moiré structure composed of alternating hcp and fcc stacked regions[62].

In the graphene/Co/Ru(0001) system increasing the Co film thickness weakens perpendicular magnetic anisotropy, analogous to the findings reported in Ref. 12. This allows us to tailor the effective magnetic anisotropy of our samples by approaching the spin reorientation transition point from out-of-plane to in-plane, where the effective anisotropy can become extremely small. Proximity to the spin reorientation transition results in rather large width of the domain walls[64], which is useful for the precise mapping of domain wall spin textures in the SPLEEM.

Possible signs of Co diffusion into Ru were monitored by X ray photoelectron spectroscopy (XPS) in Co/Ru (0001) films grown by the same procedure as described above. We conducted the XPS experiment at Centro do Desenvolvimento da Tecnologia Nuclear. The measurements were carried out in an ultrahigh vacuum chamber (base pressure better than 2.0×10^{-10} mbar) using an Al Kα x-ray source with the output power set at 300 W and a VG Microtech hemispherical electron energy analyzer CLAM 2/1 VU. Normal emission scans with 50 eV pass energy were acquired. Following the Co and Ru XPS signal before and after the annealing procedure, we did not observe any evidence of Co-Ru interdiffusion (see Supplementary Fig. S.5).

Real-space imaging. In the SPLEEM system, real-space images were acquired using three orthogonal electron beam spin-alignments such that magnetic contrast along three orthogonal directions corresponds to the out-of-plane magnetization direction and two orthogonal in-plane axes[65], as shown in Supplementary Fig. S.1a-c. SPLEEM images map magnetization of the sample in the sense that intensity in each pixel represents the dot product of the spin polarization vector **P** of the illumination beam and the magnetization vector **M**. The lateral spatial resolution of the SPLEEM at Berkeley lab is ~15 nm, while the measured DW width in the systems studied here is between 150 nm to 350 nm. The energy of the incident electron beam was set to 3.6 eV for graphene/Co/Ru and 5 eV for Co/Ru; these values were chosen to optimize the magnetic contrast. All images were obtained with samples at room temperature. The images are represented in grey scale, where a black and white contrast correspond to the magnetization vector pointing into the film plane ($+M_z$) and out of the plane ($-M_z$), respectively, as shown in Supplementary Fig. S.1a, 1b and 1c. To highlight DW spin structures, the triplets of SPLEEM images representing out-of-plane and orthogonal in-plane magnetization components are combined into single compound images, as shown in Supplementary Fig. S.1e. In this projection, colours represent the in-plane magnetization as indicated by the colour wheel (inset), black and grey values represent the perpendicular magnetization component, $+M_z$ and $-M_z$, respectively.

Analysis of chirality. The method to analyse DW chirality from the SPLEEM images is the same as described by G. Chen, et al.[48] First, along all DWs the DW normal direction **n** is determined from the out-of-plane magnetization SPLEEM images, where **n** is defined as a vector pointing from spin-down ($-M_z$) to spin-up ($+M_z$) domains. Then, at all pixels along the DW centrelines, the in-plane magnetization direction, (**m**), is measured from the grey values of the two in-plane SPLEEM images. To improve the signal-noisy ratio, in this step each

pixel is averaged with its three nearest neighbour pixels. Finally, we compute the angle α, defined as the angle between **m** and **n** (inset of Fig. 3c), and we calculate its distribution along all DW centrelines, as represented by the histograms.

Estimating the exchange stiffness. The strength of the Rashba-induced DMI at graphene/Co interfaces depends on the value of the exchange stiffness, which, in very thin films, can be lower than the Co bulk value of 15 pJ/m.[34] The exchange stiffness in graphene/Co/Ru(0001) samples can be estimated from the Curie temperature, which is obtained by real-time SPLEEM measurement of the temperature dependent magnetization. The Curie temperature T_C depends on the exchange stiffness A as $T_C = \frac{2z_{NN}(g_J-1)^2 J_{ex}}{3k_B} J(J+1)$ where $A = 2\frac{J_{ex}S^2 z_{NC}}{a}$ [66], z_{NN} is the number of nearest neighbor atoms, g_J is the g-factor, k_B is the Boltzmann constant, J is the total angular momentum quantum number, S is the spin quantum number, z_{NC} is the number of atoms in a unit cell, and a is the lattice constant. For graphene/Co(3ML)/Ru(0001) we find that the Curie temperature is about 861K (see Supplementary Fig. S.6). In this sample structure $z_{NN} = 12$, $g_J = 2.09$, $k_B = 1.38 \times 10^{-23}$ m^2 kg s^{-2} K^{-1}, $J = 1/2$, $S = 1/2$, $z_{NC} = 4$, so the result $T_C^{3ML\ Co} = 861$K leads to the experimental estimate of A as $9.5\ \mathrm{pJ/m}$ for 3ML Co. Measuring thicker films we find that for graphene/Co(4 ML)/Ru the magnetic contrast remains strong up to above 943K, but in this temperature range the films are not stable. Thus a lower limit of A in graphene/Co(4 ML)/Ru can be estimated as $10.4\ \mathrm{pJ/m}$ and an upper limit of the exchange stiffness in films of any thickness is the value of bulk Co, 15 pJ/m.

Estimating the DMI strength. The orientation of magnetization within the domain wall with respect to the domain boundary direction in Fig. 3 allows one to estimate the strength of the interfacial DMI, using methods described in more detail in refs. 36 and 48. Briefly, the free

energies of Néel and Bloch walls can be written as $E^{\text{Néel}} = E_{\text{EX}}^{\text{Néel}} + E_{\text{A}}^{\text{Néel}} + E_{\text{d}}^{\text{Néel}} + E_{\text{DM}}^{\text{Néel}}$ and $E^{\text{Bloch}} = E_{\text{EX}}^{\text{Bloch}} + E_{\text{A}}^{\text{Bloch}} + E_{\text{d}}^{\text{Bloch}} + E_{\text{DM}}^{\text{Bloch}}$ respectively, where E_{EX}, E_{A}, E_{d} and E_{DM} correspond to exchange energy, magnetic anisotropy energy, dipolar energy and DMI energy of the walls, respectively. Néel wall is favoured when $E^{\text{Néel}} < E^{\text{Bloch}}$; and since both the exchange and magnetic anisotropy energy are degenerate for Néel- and Bloch-type walls and the interfacial DMI energy vanishes for Bloch-type walls[49], this inequality can be expressed as $E_{\text{d}}^{\text{Néel}} + E_{\text{DM}}^{\text{Néel}} < E_{\text{d}}^{\text{Bloch}}$. Likewise, Bloch wall is favoured when $E_{\text{d}}^{\text{Néel}} + E_{\text{DM}}^{\text{Néel}} > E_{\text{d}}^{\text{Bloch}}$. Thus, from observations of thickness-dependent transitions from Néel to Bloch wall, the range of $E_{\text{DM}}^{\text{Néel}}$ can be bracketed by computing the dipolar energy contributions. Samples with thickness below the wall-type transition feature Bloch walls and $E_{\text{d}}^{\text{Bloch}} - E_{\text{d}}^{\text{Néel}} < E_{\text{DM}}^{\text{Néel}}$, whereas in samples with thickness above the transition walls have Néel structure and $E_{\text{DM}}^{\text{Néel}} < E_{\text{d}}^{\text{Bloch}} - E_{\text{d}}^{\text{Néel}}$. Using the method for calculating the dipolar energy difference as described in refs. 36 and 48, the dipolar energy constant D_{dip} is $\frac{\mu_0 (\text{d}_{\text{Co}} \mu_{\text{Co}})^2}{8\pi a_{\parallel}^3}$ [48], where $\mu_0 = 4\pi \times 10^{-7} \text{H} \cdot \text{m}^{-1}$, $\mu_{\text{B}} = 9.27 \times 10^{-24}\ \text{A} \cdot \text{m}^2$, $\mu_{\text{Co}} = 1.7\mu_{\text{B}}$, $a_{\parallel} = 2.51$Å. Using the Matlab software, we numerically calculate the dipolar energy difference $E_{\text{d}}^{\text{Bloch}} - E_{\text{d}}^{\text{Néel}}$ of graphene/Co/Ru(0001) with various thicknesses. In graphene/Co/Ru(0001) films, observations of Néel walls for Co=3.9ML, titled walls for Co=4.8ML, and Bloch-like walls for Co=5.7ML lead to values of $E_{\text{d}}^{\text{Bloch}} - E_{\text{d}}^{\text{Néel}} = -0.38$ meV per atom, -0.58 meV per atom and -0.81 meV per atom, respectively. Note that the dipolar energy cost of Néel walls $E_{\text{d}}^{\text{Néel}}$ is greater than that of Bloch walls $E_{\text{d}}^{\text{Bloch}}$ [36,48], therefore all numbers calculated above are negative. In the calculation, the width of domain walls is chosen as 150nm, which is consistent with estimates of both Néel and Bloch walls observed in the SPLEEM images. For a hexagonal lattice, $E_{\text{DM}}^{\text{Néel}} = -\sqrt{3}\pi d$, [48] where d is the

magnitude of the DMI vector. Therefore d in graphene/Co/Ru(0001) system can be estimated as $d = 0.11 \pm 0.04$ meV per atom. Similarly, d in Co/Ru system can be estimated as $d = -0.05 \pm 0.01$ meV per atom based on 3ML Co/Ru result (Fig. 3e) where roughly 45° titled magnetization with respect to the domain boundary (see two peaks at 135° and 225° in Fig. 3e) indicates that the dipolar energy difference between Néel- and Bloch- DWs $E_{\mathrm{d}}^{\mathrm{Bloch}} - E_{\mathrm{d}}^{\mathrm{Néel}}$ is comparable to the DMI energy $E_{\mathrm{DM}}^{\mathrm{Néel}}$. Here the error bar is given by the uncertainty of the magnetization profile within in-plane region[36]. Therefore, d at graphene/Co interface with Co thickness ranged from 4-6 ML can be estimated as 0.16 ± 0.05 meV per atom, based on the estimated d values in graphene/Co/Ru(0001) and in Co/Ru(0001).

Data availability. The data that support the findings of this study are available from the corresponding authors upon reasonable request.

[56] Kresse, G. & Hafner, J. Ab initio molecular dynamics for liquid metals. *Phys. Rev. B* **47**, 558–561 (1993).
[57] Kresse, G. & Furthmüller, J. Efficient iterative schemes for ab initio total-energy calculations using a plane-wave basis set. *Phys. Rev. B* **54**, 11169–11186 (1996).
[58] Xiang, H. J., Kan, E. J., Wei, Su-Huai, Whangbo, M.-H. & Gong, X. G. Predicting the spin-lattice order of frustrated systems from first principles. *Phys. Rev. B* **84**, 224429 (2011).
[59] Bihlmayer, G., Kroteev, Y. M., Echenique, P. M., Chulkov, E. V. & Blugel, S. The Rashba-effect at metallic surfaces. *Surface Science* **600**, 3888 (2006).
[60] Sutter, P. W., Flege, J.-I. & Sutter, E. A. Epitaxial graphene on ruthenium. *Nature Mater.* 7, 406–411 (2008).
[61] Huang, L. et al., Intercalation of metal islands and films at the interface of epitaxially grown graphene and Ru(0001) surfaces. *Appl. Phys. Lett.* **99**, 163107 (2011).
[62] El Gabaly, F. et al. Structure and morphology of ultrathin Co/Ru(0001) films. *New J. Phys.* **9**, 80 (2007)
[63] Liao et al. Intercalation of cobalt underneath a monolayer of graphene on Ru(0001). *Surf. Rev. Lett.* **19**, 1250041 (2012).
[64] Hubert, A. & Schäfer, R. Magnetic Domains (Springer, Berlin, 1998).
[65] Chen, G. et al. Out-of-plane chiral domain wall spin-structures in ultrathin in-plane magnets. *Nat. Commun*. **8**, 15302 (2017).
[66] Blundell, S. J. Magnetism in Condensed Matter (Oxford University Press, Oxford, 2001).